JOURNAL OF MATERIALS SCIENCE 15 (1980) 73–81

Mictomagnetism in a new $BaO.Fe_2O_3.B_2O_3$ glass

H. LAVILLE, J. C. BERNIER
Département Science des Matériaux ENSCA, ERA 679 du CNRS, 1, rue Blaise Pascal, B.P. 296/R8, 67008 Strasbourg Cedex, France

An homogeneous $BaO \cdot Fe_2O_3 \cdot B_2O_3$ glass containing 30% Fe_2O_3 is prepared by a splat-cooling technique. X-ray and electron diffraction reveal the product to be amorphous at room temperature. The crystallization, as shown by DTA studies, begins at 750 K, and up to 950 K, a temperature at which $BaFe_{12}O_{19}$ is shown to be present, the crystallizing products are mainly evolutive.

The magnetic measurements show a probably mictomagnetic behaviour at low temperature with a maximum of magnetic susceptibility at 12 (±1) K. At higher temperature the susceptibility obeys a Curie–Weiss law with large negative Weiss constant and low Curie constant per Fe^{3+} ions. After crystallization the product is ferrimagnetic and could be used as a permanent magnet.

Mössbauer study reveals that the glass mainly consists of Fe^{3+} ions in distorted sites and a hyperfine structure at low temperature; the magnetic ordering temperature is estimated to be about 44 (±1) K.

1. Introduction

In order to study the amorphous state in ionic solids, the class of oxide-based materials generally referred to as glass proves of great interest. The $BaO \cdot Fe_2O_3 \cdot B_2O_3$ compositions have been widely studied [1–5], but, as the preparation in the amorphous form of samples with high Fe_2O_3 content is impossible by the ordinary glass-forming technique, we used a splat-cooling technique.

The splat-cooling techniques, initiated by Duwez [6], allow quenching from the melt at rates estimated to be as high as 10^6 to 10^8 K sec^{-1} [6]. The methods, initially limited to metallurgy [7, 8] have been extended to pure oxides [9, 10] and mixed oxides [11–13] and it appears clearly from these works that the quench is better when the compositions are close to those of binary or ternary eutectics and when one adds a network former such as SiO_2, B_2O_3 [1, 14, 15] or a network modifier such as Na_2O [16].

In the present study we succeeded in obtaining an homogeneous glass containing 30% Fe_2O_3 by cooling on rollers.

2. Experimental details

Splat-cooling on rollers is a well known technique which has been described several times [15, 17, 18] and has here been adapted to our products.

The oxides are generally electric insulators, so they are heated and melted indirectly by induction in a metallic crucible. The disadvantage of the Pt–30% Rh crucible we use is that at high temperatures a great part of the heat is lost by radiation. Thus it was impossible to reach the temperature at which the bath is fluid enough to run through the evacuation tube of the crucible (see crucible in Fig. 1). For this reason a composite crucible (Fig. 1) was used: the Pt–30% Rh crucible containing the oxide mixture is set into a suitably shaped graphite cylinder. The radiation coming from the metallic crucible is reflected by the graphite; higher temperatures are attainable and so the initial mixture can be properly melted. The composite crucible is suspended by means of tungsten wires (2 or 3) connected to a vertical refractory oxide tube (Fig. 2). To prevent the burning of graphite in air when heated, the oxidation of tung-

0022–2461/80/010073–09$02.90/0

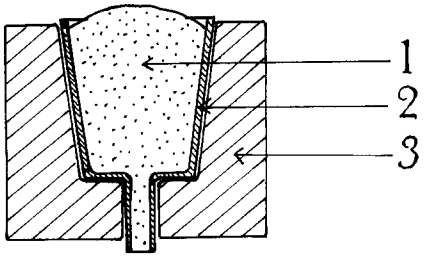

Figure 1 Composite crucible: 1. Oxide mixture; 2. Pt–Rh 30% crucible; 3. Graphite cylinder.

sten wires, and also a possible reduction of Fe^{3+} ions due to the reactivity of graphite, we worked in an inert flowing atmosphere of argon (the flow was approximately 10 litre min^{-1}).

In order to quench we used two steel rollers weighing 1 kg each and rotating at 3000 rev min^{-1} The advantage of steel is that, though it is less conductive of heat than the brass or bronze generally used, it is harder. So the roller surface is not damaged by the first molten droplets which sometimes still contain some crystallites. Thus the contact between the two rollers remains good and the result is that the thickness of the ribbons is constant and small ($\simeq 50\,\mu m$) so that the quench is very good.

Scrapers were used to separate the ribbons from the rollers and baffles to prevent them from flying away. Fig. 3 shows the whole apparatus and Fig. 4a and b some of the ribbons obtained.

The B_2O_3 25% ·BaO 45% ·Fe_2O_3 30% composition was chosen. Starting materials for splat-cooling were prepared by mixing $BaCO_3$ and H_3BO_3 in appropriate proportions and heating slowly from 300 to 1050 K to allow the different products to react without losing any B_2O_3 by evaporation, (which was checked by weighing). The mixture of barium borates obtained was milled and mixed with Fe_2O_3 in appropriate proportions and heated at 1050 K for some hours. The resulting product was then melted and extruded between the rollers.

The thin ribbons obtained were sorted by means of a 3000 Oe magnet. Only the "non-ferromagnetic" part was kept for the measurements.

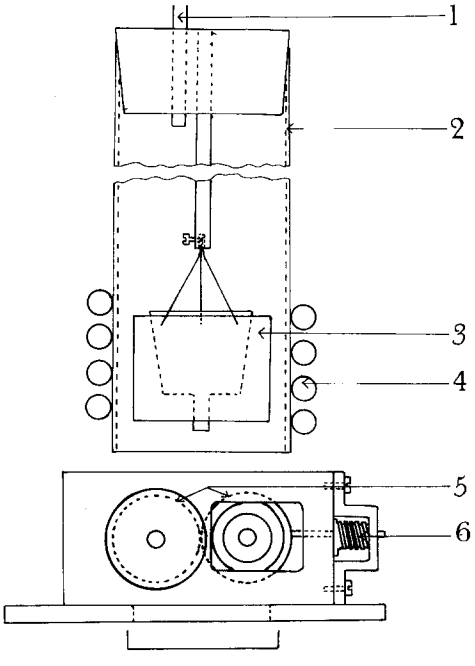

Figure 2 Scheme of the apparatus used for splat cooling: 1. Tube for gas arrival; 2. Silica tube; 3. Composite crucible; 4. Induction coil; 5. Rollers; 6. Spring to allow a good contact between the rollers.

3. Chemical analysis

The composition was checked because during the melting process vapours are lost. We checked the iron and barium content by spectrometric methods after dissolution of the sample in dilute hydrochloric acid.

The iron content was checked by measuring the absorption of the red iron thiocyanate complex [19] prepared in hydrochloric acid. The calibration curve was obtained by preparing some complexes with definite quantities of the initial powders prepared for the splat-cooling experiments, as the complex is not very stable the measurements are made after a well defined time.

The barium content was measured by colorimetry of CrO_4^{2-} [20]. To a definite sample in hydrochloric acid we add an excess of a standardised $(NH_4)_2CrO_4$ solution. Then it was necessary to add 2 or 3 ml of concentrated NH_4OH in order to have a basic solution and precipitate $BaCrO_4$ and $Fe(OH)_3$. The sample was then filtered and the absorption of the resulting liquid measured. Once more a calibration curve was obtained by means of the powder used in splat-cooling experiments.

The results of the quantitative analysis are collected in Table I. The fact that the amount of Fe and Ba increases in the same proportion

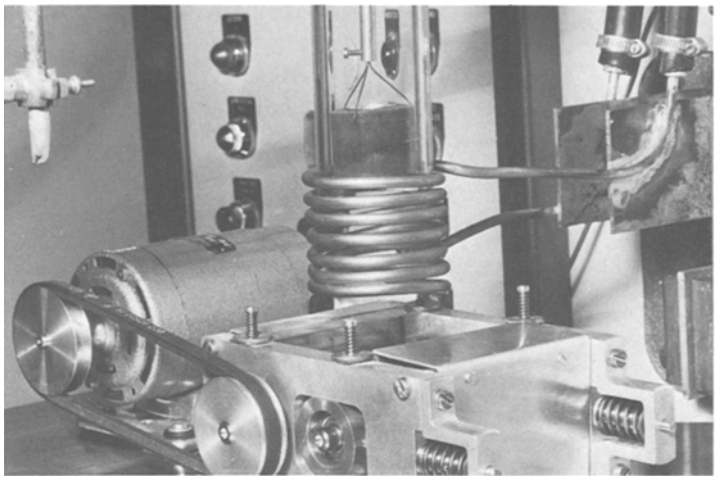

Figure 3 Splat cooling rollers.

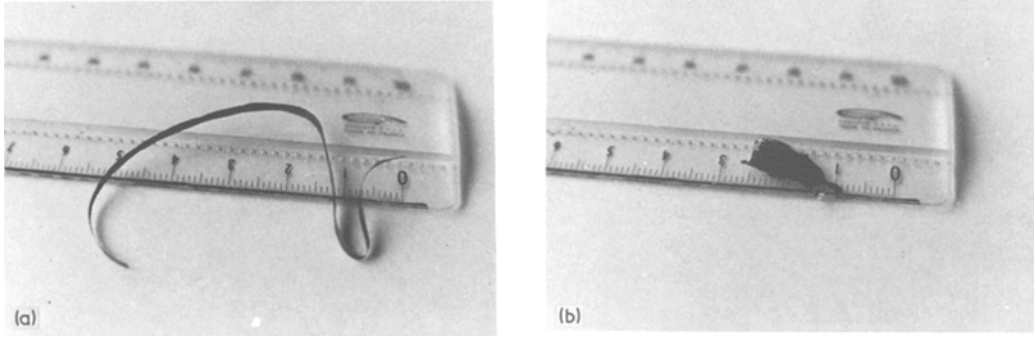

Figure 4 (a) and (b). Examples of amorphous ribbons.

(%Fe/%Ba = constant) suggests that the differences were due to B_2O_3 evaporation, so that the product obtained is poorer in B_2O_3 than expected.

The calculations lead to the information presented in Table I.

4. Physical analysis

The amorphous products were investigated by X-ray and electron diffraction. X-ray diffraction results pointed to a non-crystalline structure. The electron diffraction confirmed that besides a few very small crystallites the samples were essentially amorphous. Figs. 5 and 6 show the TEM micrograph of an amorphous sample and the corresponding electron diffraction pattern.

TABLE I Results of the quantitative analyses

Component	Theoretical (wt%)	Measured (wt%)	% Meas − % th / % th
Fe	24.95	25.6	+ 0.026
Ba	46.01	47.15	+ 0.025

Differential thermal analysis (Fig. 7) shows a complex pattern of crystallization. The graphical recording shows four exothermic peaks (the first one beginning in an endothermic way) and an endothermic peak. In order to determine the crystalline products at any temperature, crystallizations followed by X-ray diffraction, and X-ray diffraction experiments at high temperature were performed on several specimens. It was difficult to draw conclusions from the results. The following features were established:

(1) At the temperature of the first DTA peak there appears momentarily a liquid phase (after heating at 820 K and cooling, the products seems to have been molten) and we observe only one X-ray line ($d = 3.14$ Å).

(2) A complex system of borates then crystallizes, changing with temperature.

(3) Barium hexaferrite $BaFe_{12}O_{19}$ begins to

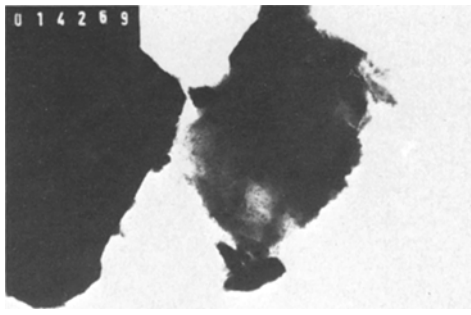

Figure 5 Electron microscopy on a sample (× 19 500).

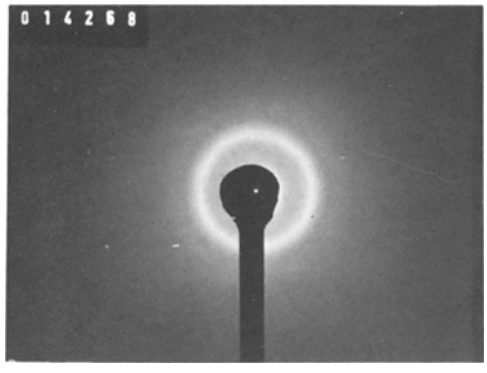

Figure 6 Electron diffraction pattern on the sample of Fig. 5.

appear at approximately 900 K but, as the crystallites are very small, the X-ray lines are very weak and diffuse; so it is not possible to specify the exact temperature of the $BaFe_{12}O_{19}$ crystallization. But this result is close to a result obtained on a $BaO{\cdot}Fe_2O_3{\cdot}Na_2O$ glass [16]. At 980 K, the crystallized system composed of different crystalline products is very complex. Fig. 8a and b, which show the electron diffraction patterns after heating to this temperature, give an idea of this complexity.

(4) Above 1030 K, the borate system changes radically and probably melts while $BaFe_{12}O_{19}$ develops.

5. Magnetic properties

The magnetic measurements were carried out on a Foner magnetometer [21] below room temperature and on a balance of the Faraday type above room temperature. They showed several interesting facts.

The magnetization curves at room temperature reveal the linear dependence of magnetization on field (Fig. 9) with a very weak ferromagnetic component, probably due to an imperfect magnetic sorting at the lower fields. At 4.2 K the magnetization curves (Fig. 11) depend on the way the sample has been cooled. When cooled without field the product behaves like a true paramagnetic material; field-cooled ($H = 18.8$ kOe) the magnetization at zero defines the thermomagnetic remanence at 4.2 K but we have to note that the susceptibility ($\chi = d\sigma/dH$) remains constant. This thermomagnetic remanence disappears above 14 K. This field-cooling treatment gives rise to an hysteresis loop displaced with respect to the zero of the field (Fig. 10). But when the sample is cooled in a field perpendicular to the measuring field the thermomagnetic remanence does not appear and there is no longer a hysteresis loop.

Fig. 11 shows the very peculiar properties observed between 4.2 and 77 K. We observe:

(1) A very broad maximum of the susceptibility measured as $d\sigma/dH$. The temperature of this maximum is approximately (12 ± 1) K.

(2) The magnetization behaviour at 18.8 kOe

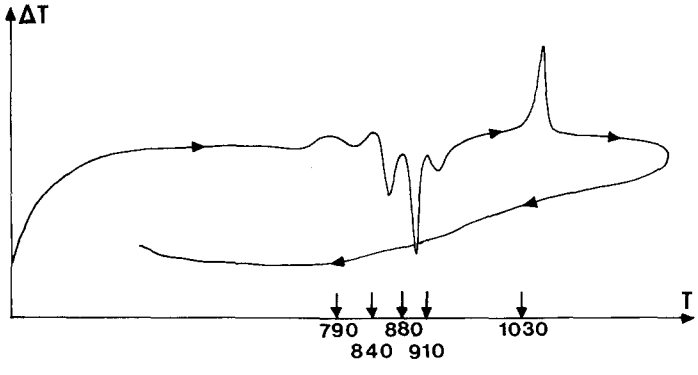

Figure 7 DTA study.

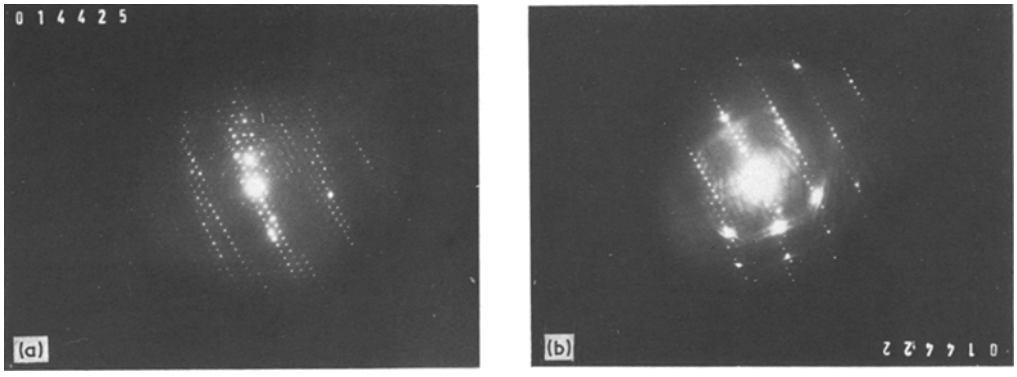

Figure 8 (a) and (b). Complexity of the sample crystallized at 980 K illustrated by electron diffraction patterns.

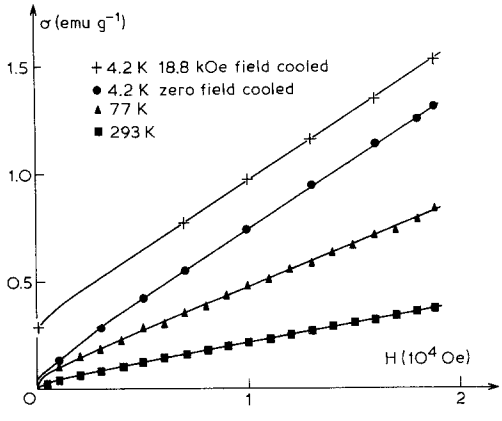

Figure 9 Magnetization curves.

versus temperature is dependent on the "field-treatment". If the sample has been cooled without field the magnetization passes through a maximum. This maximum corresponds to the susceptibility maximum already found ($T = 12 \pm 1$ K). Cooled in a 18.8 kOe field the magnetization at 4.2 K is higher and the maximum disappears. Above (14 ± 1) K the curve is the same as the one obtained when the sample is not field cooled.

This behaviour leads us to think this product could be mictomagnetic, [22, 23] where the peculiar magnetic properties are due to giant magnetic clusters.

Above 65 K the inverse of susceptibility

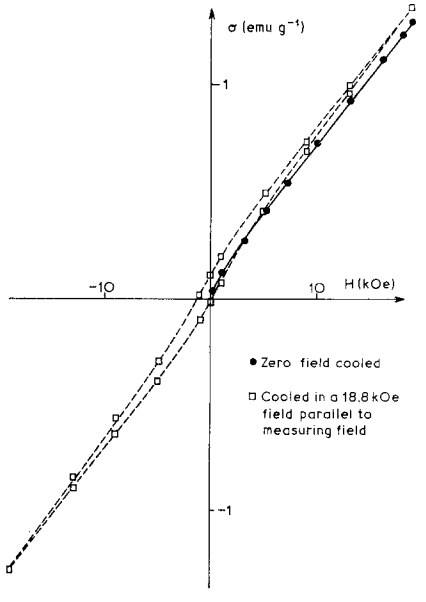

Figure 10 "Hysteresis loop" after cooling under field.

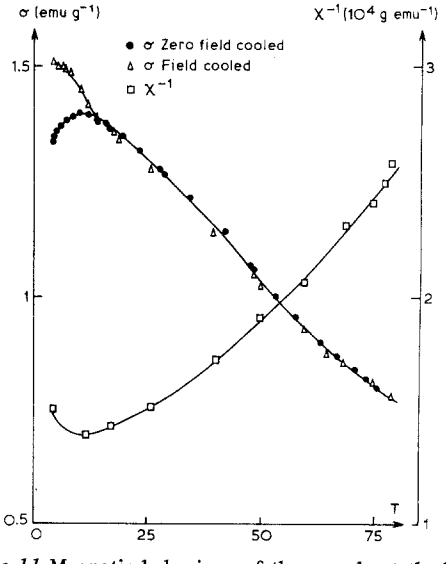

Figure 11 Magnetic behaviour of the sample at the lower temperatures.

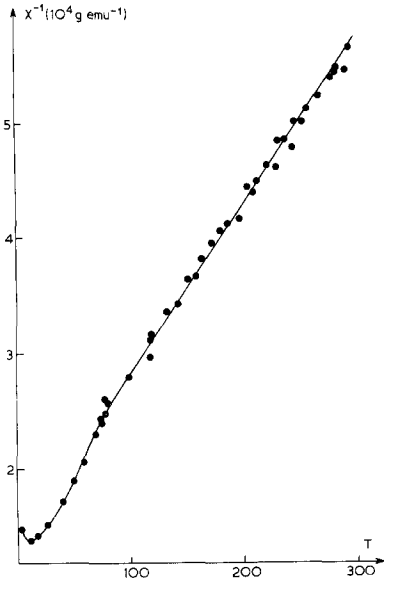

Figure 12 χ^{-1} in the temperature range 4.2 K < T < 300 K.

presents Curie–Weiss behaviour (Fig. 12) with a very weak Curie constant per ferric ion. We obtained:

$$\frac{1}{\chi} = \frac{T+95}{1.52}$$

The 1.52 value is much smaller than the theoretical one ($C = 4.37$) but similar behaviour has been found in other amorphous iron compounds [16, 24, 25]. The extrapolated Weiss constant of $\theta = (-95 \pm 2)$ K suggests rather strong antiferromagnetic interactions in the glass.

Above room temperature, as the measurements have been made on a Faraday balance type, the ferromagnetic component prevents us from knowing at what temperature the Curie–Weiss behaviour really disappears, but we observe (Fig. 13) a linear dependence of χ^{-1} on T up to 750 K.

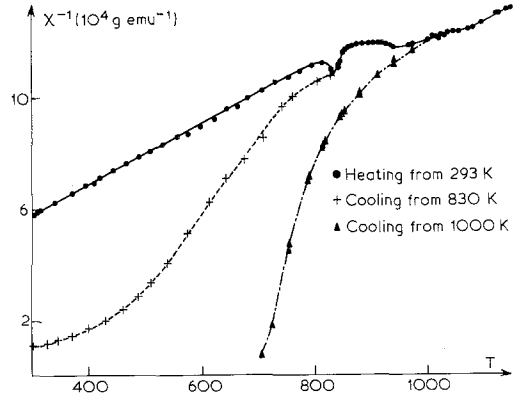

Figure 13 χ^{-1} above room temperature.

At higher temperature we observe clearly first the crystallization and then a decrease of $1/\chi$ at 820 K. We are unable to differentiate the following values, and during these crystallization χ^{-1} remains nearly constant.

Nevertheless, from studying $1/\chi$ with decreasing temperature it appears clearly that the ferrimagnetic phase does not crystallize in the course of the first crystallization (see Fig. 13, cooling from 830 K).

The hexaferrite crystallization occurs only about 900 K. As this temperature is much higher than the Curie temperature of $BaFe_{12}O_{19}$, χ remains weak. But when cooling from a temperature above this crystallization temperature, ferromagnetic behaviour appears and χ increases drastically (see Fig. 13, cooling from 1000 K). The Curie temperature ($\theta_c = 750 \pm 10$ K) confirms that this phase is barium hexaferrite.

At 1050 K the sample "melts". This temperature is somewhat higher than the temperature determined in the DTA study but this is probably due merely to the dynamic method used with DTA apparatus which introduces a temperature lag.

Magnetization measurements have also been carried on samples annealed a few minutes at various temperatures. An external field of 10 500 Oe was applied in the course of these anneals. The results are compiled in Table III.

Fig. 14 shows the evolution of the magnetization versus H at room temperature, and Fig. 15 the evolution of the hysteresis loop at room temperature.

The sample annealed at 845 K for 15 min has been particularly studied. In effect, in spite of a very weak coercive field, the magnetization versus field curve is close to the curve of a superparamagnet. So magnetization measurements have been carried out in the temperature range 4.2 K < T < 293 K. Fig. 16 shows that plotting σ versus H/T leads to a simple curve above the blocking temperature found at $T = 65 \pm 3$ K. At 4.2 K we have to note an hysteresis loop characteristic of superparamagnets below the blocking temperature [25].

TABLE II Composition of the product obtained after splat-cooling

Component	Mol%	wt%
Fe_2O_3	31.53	36.6
BaO	47.23	52.65
B_2O_3	21.24	10.75

TABLE III Magnetic behaviour of annealed samples

Annealing temperature (K)	Annealing time (h)	σ at 18 000 Oe (emu g^{-1})	σ at 10 000 Oe (emu g^{-1})	σ at $H = 0$ (emu g^{-1})	$_{\sigma}H_c$ (Oe)
290	0.50	0.393	0.238	0.027	640
385	0.50	0.398	0.244	0.031	640
515	0.50	0.397	0.242	0.030	680
645	0.50	0.395	0.239	0.031	730
715	0.50	0.390	0.237	0.030	730
780	0.50	0.432	0.263	0.031	720
815	0.50	1.265	0.858	0.037	230
835	0.17	1.677	1.228	0.027	120
845	0.25	2.280	1.800	0.004	40
860	0.50	3.040	2.610	0.037	40
870	0.50	4.130	3.580	0.810	260
895	0.50	7.690	6.830	3.050	1600
935	0.50	14.130	12.550	6.830	2800
980	0.50	16.040	14.230	8.120	3550
980	1.50	16.690	14.790	8.450	4050

We observe also that when the samples are annealed at high temperature ($T = 980$ K) the ferrimagnetic properties are rather good. This is probably due to the fact that the hexaferrite grains are still monodomains which can hardly grow by sintering since they are separated by paramagnetic bonding. Naturally the specific induction of the sample is lowered by this dilution in a paramagnetic matrix so that the induction coercitive field is much lower than the magnetization coercitive field. Nevertheless the crystallized product could be used as a weak permanent magnet since we obtained.

$$B_r = 450\,\text{G}$$

$$_{B}H_c = 390\,\text{Oe}$$

$$_{\sigma}H_c = 4000\,\text{Oe}$$

6. Mössbauer experiments

A few ^{57}Fe Mössbauer measurements were performed over the temperature range $4.2\,\text{K} < T < 300\,\text{K}$ using conventional experimental procedures. Fig. 17 shows Mössbauer spectra recorded at different temperatures. At room temperature and at 77 K the spectrum presents a quadrupole split doublet with average splitting $E_Q = 0.97$ mm sec^{-1} and isomer shift IS = 0.37 mm sec^{-1} (against iron

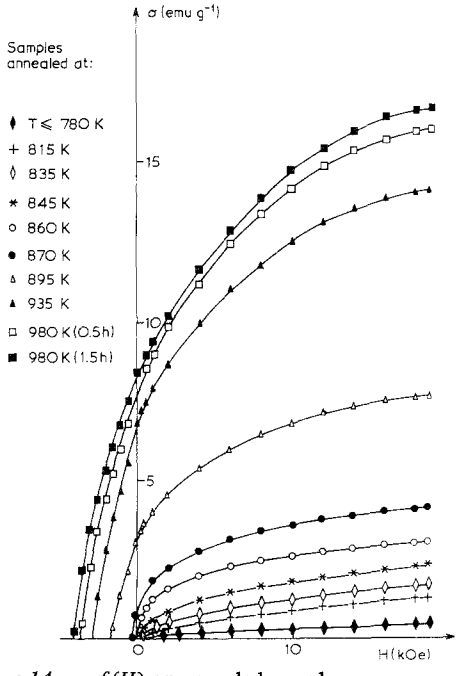

Figure 14 $\sigma = f(H)$ on annealed samples.

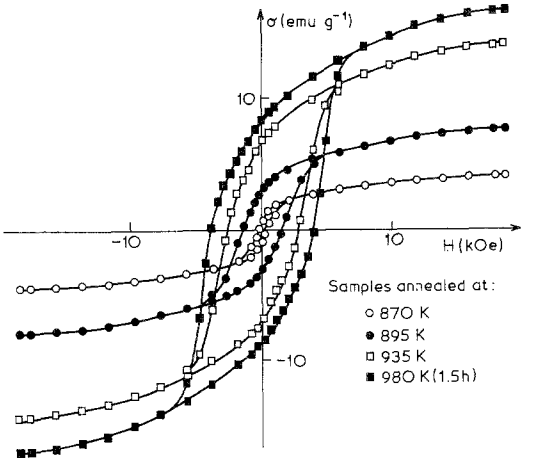

Figure 15 Hysteresis loops for samples annealed above 870 K.

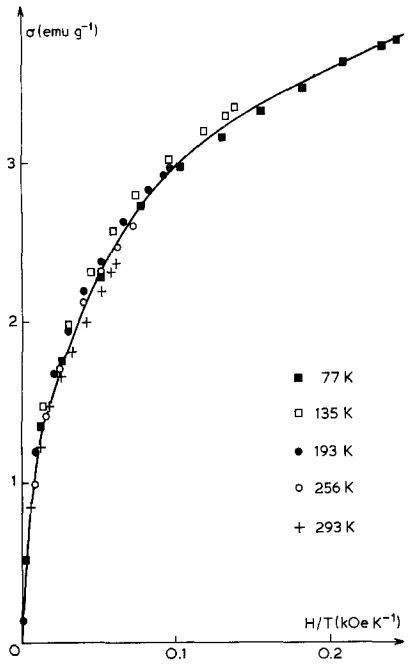

Figure 16 $\sigma = f(H/T)$ for the sample annealed at 845 K.

metal) characteristic for high spin Fe^{3+} ion in a distorted environment [27]. The broadening of the central doublet does not appear until the spectra are taken below 44 K, indicating the onset of a magnetic hyperfine splitting (hfs). At 4.2 K a six-line magnetic spectrum with an average hyperfine field $H = 430$ kOe and an apparent lack of quadrupole splitting is observed. But this six-line spectrum is not very characteristic since the width of the peaks at half height is respectively in the ratio 17/14/9. Nevertheless we can deduce from the broadened line widths observed in the paramagnetic doublet, as well as in the magnetic split spectra, that both the electric field gradient and the hyperfine field present a wide distribution in magnitude typical of amorphous magnetic solids [28].

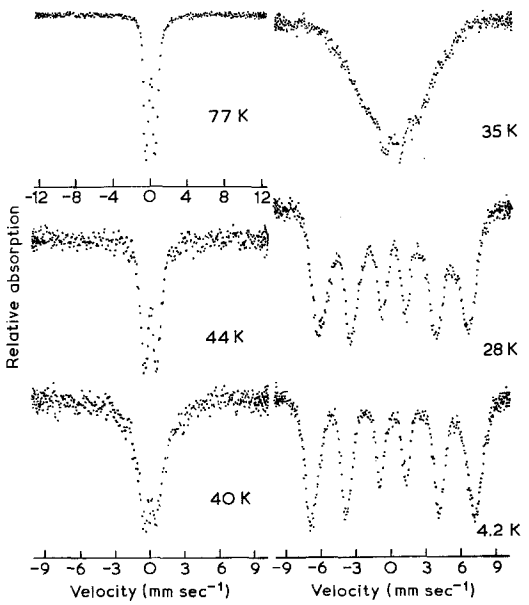

Figure 17 Temperature dependence of the Mössbauer spectra for the amorphous $BaO \cdot Fe_2O_3 \cdot B_2O_3$ glass.

7. Conclusions

The study of this amorphous system reveals several facts which are noteworthy.

(1) At ordinary temperatures the product is amorphous. The iron cations (Fe^{3+}) are in a true glass.

(2) The magnetic measurements and Mössbauer spectra taken at low temperature reveal a magnetic ordering temperature. According to Beck [29] and to the phenomena observed in crystallized metallic alloys, we suppose that the sample exhibits a paramagnetic → mictomagnetic transition. This seems to be confirmed by the action of cooling under a magnetic field which gives rise to an unidirectional remanence and consequently a displaced "hysteresis loop". It appears reasonable to think that these peculiar properties are due to magnetic clusters which can interact one with another and perhaps with the anti-ferromagnetically coupled Fe^{3+} ion of the matrix. A large distribution of size of the clusters and a similar large distribution of their relaxation time could explain the very broad range of maximum susceptibility as well as the difference between the transition temperature obtained by susceptibility measurements and Mössbauer spectra, 12 and 44 K respectively. These phenomena seem to be rather generally reported. In effect a similar behaviour has been found in a $Fe_2O_3-Li_2O-SiO_2$ glass [30]; an hysteresis loop displaced in the direction opposite to the cooling field has also been observed in a $BaO \cdot Fe_2O_3 \cdot B_2O_3$ glass [4]. The freezing of the giant moments of the magnetic clusters as a result of anisotropy has been invoked in cobalt and manganese aluminosilicate glasses [31, 32];

(3) Above 65 K the susceptibility obeys a Curie–Weiss law. The large negative extrapolated Weiss constant demonstrates the strong antiferromagnetic interactions of the iron cations. The surprisingly low Curie constant may be attributed

to the effective cancellation of an important fraction of the Fe atomic moments.

(4) The glass crystallizes at higher temperatures. Consequently in the first stage of this crystallization we observe a paramagnetic → superparamagnetic transition. The σ versus H/T single curve can be fitted by the equation $\sigma = 4.095$ [coth $(38.043\,H/T) - 0.026\,T/H$] which corresponds to $\mu = 52.5 \times 10^{-16}$ emu. As this crystallized system is an hexaferrite precursor, we assume these superparamagnetic particles are giant $BaFe_{12}O_{19}$ clusters, where the iron cations are coupled ferrimagnetically with $\mu_{Fe} = 5\,\mu_B$ results give the average size of the cluster as $D \simeq 210$ Å; this average value has been confirmed by electron microscopic observations.

Heated at higher temperature, $BaFe_{12}O_{19}$ crystallizes and the hexaferrite crystallites are large enough to give rather good ferromagnetic properties, especially a high coercive field which would allow this "vitroceram" to be used as a material for permanent magnets.

In conclusion we put emphasis on the sequence of magnetic transitions:

Mictomagnetism → paramagnetism →

superparamagnetism
↓
ferrimagnetism

However the nature of the transition, mictomagnetism → paramagnetism, is far from being solved. Susceptibility measurements at low fields could give some useful information and, if a sharp cusp in the low-field susceptibility is a criterion, could answer the question whether this product is a spinglass or not.

Acknowledgement

The authors are grateful to J. M. Friedt for the Mössbauer measurements.

References

1. B. T. SHIRK and W. R. BUESSEM, *J. Amer. Ceram. Soc.* **53** (1970) 192.
2. M. FAHMY, J. J. PARK, M. TUMOZAWA and R. K. MacCRONE, *Phys. Chem. Glasses* **13** (1972) 21.
3. D. W. MOON, J. M. AITKEN, R. K. MacCRONE and G. S. CIELOSZYK, *ibid.* **16** (1975) 91.
4. M. J. PARK and R. K. MacCRONE, *J. Korean Phys. Soc.* **7** (1974) 73.
5. H. TANIGAWA and H. TANAKA, *Osaka Kogyo Oyutsu Shikenoko Kiko*, **15** (1964) 285.
6. P. DUWEZ, *J. Appl. Phys.* **31** (1960) 1136
7. H. JONES, G. SURYANARAYANA, *J. Mater. Sci.* **8** (1973) 705.
8. G. H. GOKULARATHNAM, *ibid.* **9** (1974) 673.
9. P. T. SARJEANT and R. ROY, *J. Amer. Ceram. Soc.* **50** (1967) 500.
10. P. KANTOR, A. REVCOLEVSCHI and R. COLLONGUES, *J. Mater. Sci.* **8** (1973) 1359.
11. T. SUZUKI and A. M. ANTHONY, *Mater. Res. Bull.* **9** (1974) 745.
12. J. B. MONTEIL, J. C. BERNIER and A. REVCOLEVSCHI, *ibid.* **12** (1977) 235.
13. J. B. MONTEIL, L. PADEL and J. C. BERNIER, *J. Solid State Chem.* **24** (1978) 134.
14. O. HORIE, Y. SYONO, Y. NAKAGAWA, A. ITO, K. OKAMURA and S. YAJIMA, *Solid State Comm.* **25** (1978) 423.
15. C. CHAUMONT, J. BOISSIER and J. C. BERNIER, *Rev. Int. Htes Temp. Réfract.* **15** (1978) 23.
16. H. LAVILLE, J. C. BERNIER, J. P. SANCHEZ *Sol. State Comm.* **27** (1978) 259.
17. A. REVCOLEVSCHI, *Revue de la Société d'Encouragement pour l'Industrie Française* **1** (1974) 3.
18. H. S. CHEN and C. E. MILLER, *Rev. Sci. Instrum.* **41** (1970) 1237.
19. G. CHARLOT, "Chimie Analytique Quantitative" (Masson, Paris, 1974) p. 413.
20. S. CHRISTOW, *Z. Anal. Chem.* **125** (1943) 278.
21. S. FONER, *Rev. Sci. Instrum.* **30** (1959) 548.
22. S. CHAKRAVORTY, P. PANIGRAHY and P. A. BECK, *J. Appl. Phys.* **42** (1971) 1698.
23. H. OESTERREICHER, *J. Solid State Chem.* **26** (1978) 33.
24. J. M. D. COEY, P. W. READMAN, *Nature* **246** (1973) 476.
25. J. M. D. COEY, *Phys. Bull.* **27** (1976) 294.
26. L. NEEL, *Ann. Geophysique* **5** (1949) 99.
27. J. M. D. COEY, *J. Phys. (Colloque)*, **35** (1974) 89.
28. T. E. SHARON and C. C. TSUEI, *Phys. Rev. B* **5** (1972) 1047.
29. P. A. BECK, *Prog. Mater. Sci.* **23** (1978) 1.
30. G. R. MATHER, "Amorphous Magnetism" (Plenum Press, New York, 1973) p. 87
31. R. A. VERHELST, R. W. KLINE, A. M. De GRAAF and H. O. HOOPER *Phys. Rev.* **B11 (1975)** 4427.
32. L. A. BIEMAN, P. F. KENEALY and A. M. De GRAAF, "Amorphous Magnetism II" (Plenum Press, New York, 1977) p. 587.

Received 13 March and accepted 28 March 1979.